Turkish Journal of Physics

http://journals.tubitak.gov.tr/physics/

Research Article

Turk J Phys
(2020) 44: 539 – 553

doi:10.3906/fiz-2006-13

# Dispersion management for optical parametric amplifiers in midinfrared

**Hüseyin ÇANKAYA***
Department of Physics and the Hamburg Centre for Ultrafast Imaging, University of Hamburg, Hamburg, Germany

**Received:** 30.06.2020 • **Accepted/Published Online:** 04.11.2020 • **Final Version:** 18.12.2020

**Abstract:** Midinfrared (MIR) is an attractive spectral region for many applications ranging from vibrational spectroscopy to attosecond physics. However, in this spectral region, the dispersion management techniques are not as mature as the ones in the near-infrared (NIR) or visible, which is a key ingredient of ultrafast laser technology. In this manuscript, the transfer of dispersion management schemes for optical parametric (chirped pulse) amplifiers (OP(CP)As) from NIR to MIR is discussed. Among those, a scheme based on Martinez-type grating stretcher and a bulk compressor is proposed and numerically analyzed. As a case study, the proposed scheme is applied numerically to a 2-µm pumped two-stage optical parametric amplifier (OPA) system at 4.06 µm. In the model OPA system, the seed pulses are generated by white-continuum in bulk crystal and then amplified via zinc germanium phosphide (ZGP)-based OPAs. Parametric gain bandwidth of the ZGP nonlinear crystal is numerically studied. According to the numerical simulations, 3-mm crystal supports pulses with 26.5 fs pulse duration (FWHM) at 4.06 µm. With the proposed dispersion management scheme, the seed pulses are first stretched inside a Martinez grating stretcher to 1.4–1.6 ps for efficient amplification in OPA stages and then compressed down to the transform-limit inside $CaF_2$ bulk material.

**Key words:** Ultrafast optics, ultrafast amplifiers, nonlinear optics, midinfrared lasers, ultrafast pulse shaping, optical parametric amplifiers

## 1. Introduction

In recent years, there has been a high demand for high-energy, high-repetition-rate, ultrafast midinfrared (MIR) laser sources in the spectral range between 2.5 and 10 µm for complex experiments in attosecond science and strong-field physics [1–5]. Few solid-state laser systems can generate ultrafast laser pulses directly in this spectral region without any frequency shift, namely $Cr^{2+}$ and $Fe^{2+}$ doped ZnSe, ZnS, ZnTe, CdS, CdSe [6–9]. These gain media have smooth emission spectra in the range of 2.5–5 µm which are highly suitable for mode-locked operation [10–15]. However, the energy scaling of the pulses in these gain media is challenging due to the relatively short upper state lifetime, strong thermal lensing, and high nonlinear refractive index. Parametric down-conversion is an alternative method to generate MIR photons from visible or NIR photons, via difference-frequency generation, optical parametric oscillation, and optical parametric amplification. To obtain high-energy MIR pulses, a strong ultrafast laser amplifier system is required to pump an optical parametric amplifier (OPA) or optical parametric chirped-pulse amplifier (OPCPA). In the NIR spectral region, laser amplifier systems for pumping OPAs are well developed and even commercially available such as Ti:Sapphire and Nd, Yb ion-based amplifier systems. These amplifier systems are used for pumping well-developed oxide-based nonlinear crystals [16–18]. However, parametric amplification inside these crystals is limited to ~4 µm due to the transparency

*Correspondence: huseyin.cankaya@cfel.de

range of the crystals. Moreover, it is not energetically favorable due to the large energy difference between the pump and the signal photons.

Development of nonoxide crystals such as zinc germanium phosphide (ZGP) (covering 2–8 µm) and optically patterned gallium arsenide OP-GaAs (covering 2–12 µm) is very noteworthy for MIR pulse generation due to higher conversion efficiency and broadband phase matching enabling short pulses [19–21]. These crystals are not transparent in the NIR and hence require pumping above 2 µm. Recent progresses in Ho ion-based ultrafast amplifier systems [20,22–24] allow direct pumping of OPAs to amplify the pulses in MIR [22,25–27].

Dispersion management is one of the key components enabling amplification of high energy pulses in any type of laser amplifier system. For OPA and OPCPAs in the NIR spectral region, dispersion management techniques are very well developed. In this spectral region, all optical materials including air pose positive group delay dispersion (GDD) and third-order dispersion (TOD) which can be compensated by using either standard prism pairs [28,29] or custom double chirped mirrors (DCMs) [30,31] or grism pair in the case of OPCPAs where relatively large stretching is required to match the seed pulses with long pump pulses (ps-ns) [32,33]. Furthermore, in this spectral region, more advanced and flexible dispersion management techniques have been employed to manipulate the dispersion via ultrafast pulse shapers based on liquid crystal technology [34] or acousto-optic modulators [35]. Even though ultrafast pulse shapers provide flexible solutions, they are complex to implement and cost-ineffective. Therefore, dispersion schemes comprising DCMs or prism pairs are a popular choice for OPAs in NIR. It is challenging to transfer those schemes directly in the MIR spectral region due to the negative sign of GDD accumulated during the propagation of pulses in most of the common optical materials. Previously, Sanchez et al. implemented a dispersion management scheme based on Martinez-type grating stretcher and $BaF_2$ bulk compressor allowing 118 fs pulses at 7 µm [26]. Malevich et al. implemented a complicated and cost-ineffective dispersion management scheme in the MIR spectral region based on acousto-optic modulator pulse-shaper technology. In this study, the pulses could be compressed down to 980 fs, whereas the transform-limited pulse duration was 60 fs [25]. In 2018, Bock et al. implemented again a cost-ineffective pulse shaper, which is based on liquid crystal technology, accompanied with bulk material in the dispersion management. They could obtain pulses as short as 80 fs in the MIR spectral region [27]. In this manuscript, a simple and cost-effective dispersion management scheme in the MIR will be proposed and numerically studied. This scheme will enable pulses with 26.4 fs pulse duration at 4.06 µm which is three orders of magnitude shorter than the record value in this spectral region. In the first part of the manuscript, the transfer of dispersion management schemes for OP(CP)As from NIR to MIR will be discussed. Among those schemes, the most promising scheme, which is based on a Martinez grating stretcher and a bulk material compressor, will be numerically analyzed and applied to a model OPA system supporting 26.4 fs pulses at 4.06 µm. In the second part of the manuscript, three different dispersion management schemes in the MIR spectral region will be discussed. The calculations for dispersion and gain spectra of the ZGP-based OPA will then be explained. In the third part, the described calculations will be applied to the model ZGP-based OPA system and the numerical results will be discussed.

## 2. Methods and analysis

### 2.1. Dispersion management schemes

As mentioned before, the dispersion management in the MIR spectral region is challenging due to the negative sign of GDD accumulated during the propagation inside the most common optical materials. Table 1 summarizes GDD, TOD, and the ratio between TOD and GDD of the most common optical materials and OPA gain media

transparent in the MIR spectral region. As a side note, those materials are chosen due to their commercially availability with large apertures and good optical qualities. The GDD and TOD at 4.06 µm from those materials during the propagation are calculated using the Sellmeier equations of the materials given in the corresponding references. As can be seen from the table, only a few materials exhibit positive GDD such as Si, Ge, ZnSe, and ZGP. Among them, only ZnSe has a zero (at ~4.83 µm) in the spectral region in interest, which makes it impractical in the dispersion management. Si and Ge provide positive GDD with low TOD-to-GDD ratio, which makes them proper candidates in a dispersion management scheme where positive GDD is required. However, the nonlinear coefficient of those crystals is relatively high with respect to the other materials; hence, the peak intensity of the pulse should be low enough to avoid an accumulation of undesired nonlinearity. $TeO_2$ provides the highest negative GDD and positive TOD, which would be very practical for the OPCPA case where the seed pulses are stretched to the pulse duration range from 10 ps to a few ns range. However, the ratio between TOD and GDD is very high (–56), which makes it challenging to compensate with a prism-, grating-, and grism-based dispersion management schemes. On the other hand, fluoride-based optical materials ($CaF_2$, $BaF_2$, $MgF_2$) possess slightly lower TOD-to-GDD ratio with respect to Sapphire and $LiNbO_2$, which makes fluorides the choice of material for dispersion management in our particular study.

**Table 1**. Dispersion parameters of some materials transparent at 4.06 µm.

| **Material** | **GDD/mm [fs$^2$/mm]** | **TOD/mm [fs$^3$/mm]** | **TOD/GDD [fs]** | **Reference** |
|---|---|---|---|---|
| $TeO_2$ | –62,464 | 3,498,139 | –56.00 | [44] |
| YAG | –1152 | 9773 | –8.48 | [45] |
| ZnSe | 69 | 751 | 10.83 | [46] |
| Si | 382 | 820 | 2.15 | [47] |
| $LiNbO_2$ (ord. -axis) | –1946 | 16,226 | –8.34 | [48] |
| $LiNbO_2$ (ex.-ord. -axis) | –1643 | 13,771 | –8.38 | [48] |
| Sapphire (ord. -axis) | –1708 | 14,376 | –8.42 | [49] |
| Sapphire (ex.-ord. -axis) | –1615 | 13,223 | –8.19 | [49] |
| Ge | 1081 | 2789 | 2.58 | [50] |
| $CaF_2$ | –296 | 2123 | –7.17 | [51] |
| $BaF_2$ | –147 | 1060 | –7.20 | [51] |
| $MgF_2$ | –440 | 3319 | –7.54 | [52] |
| ZGP (ord. -axis) | 189 | 1266 | 6.70 | [53] |
| ZGP (ex.-ord. -axis) | 252 | 1317 | 5.23 | [53] |

As shown in Table 1, pulses in the MIR spectral region accumulates positive TOD during propagation inside the materials listed in the table. To compress the stretched MIR pulses after the propagation inside those materials, a dispersion management scheme offering positive TOD is required. Table 2 summarizes three dispersion management options including dispersion management methods delivering negative TOD. The first option comprises material dispersion with negative GDD and positive TOD and a Martinez-type grating pair which provides positive GDD and negative TOD [36]. In this scheme, the Martinez grating pair will be employed as a stretcher because of relatively high loss which can be compensated during pulse amplification in OPA/OPCPA. When the angle of incidence on the grating pair is tuned, TOD-to-GDD ratio can be adjusted to match with the ratio in the compressor. As the second option, the materials are chosen to provide positive

GDD as opposed to the first option. Then the material dispersion is compensated by using a prism pair which provides both negative GDD and TOD. However, in prism pair configuration, the tuning range of TOD-to-GDD ratio is not as flexible as Martinez grating pair unless multiple prism pairs with different geometries are employed [37], which brings complexity to the dispersion management. As the third option, the prism pair is replaced by a grism pair. In this scheme, the grism pair provides negative GDD and TOD with tuning capability of TOD-to-GDD ratio covering a relatively large range in comparison to prism pair without any complicated prism pair sequence [33,37]. In order to get negative TOD, a grism pair is required in which a grating is directly manufactured over a prism, whereas a grism design based on a simple combination of grating and a prism would offer only positive TOD [33,38]. Therefore, the third option requires custom design optics. On the other hand, the first option offers a tunable ratio of TOD to GDD with commercially available on-shelf optical components. Among all three dispersion management options, the first one will be the choice of this study because the Martinez grating pair offers flexible GDD and TOD adjustment with simple optical components.

**Table 2**. Dispersion management options and corresponding signs of GDD and TOD.

| **Option 1** | | | **Option 2** | | | **Option 3** | | |
|---|---|---|---|---|---|---|---|---|
| **Device** | **GDD** | **TOD** | **Device** | **GDD** | **TOD** | **Device** | **GDD** | **TOD** |
| Material | (–) | (+) | Material | (+) | (+) | Material | (+) | (+) |
| Martinez Grating Pair | (+) | (–) | Prism Pair | (–) | (–) | Grism Pair | (–) | (–) |

### 2.2. Dispersion calculations

A dispersive device imprints a frequency-dependent phase shift over a pulse. This can be expressed as the Taylor series expansion centered around the carrier frequency $\omega_0$ as follows:

$$\phi(\omega) = \phi_0 + \phi_1(\omega - \omega_0) + \phi_2(\omega - \omega_0)^2 + \phi_3(\omega - \omega_0)^3 + \dots \quad , \tag{1}$$

where the coefficients $\phi_n$ are expressed as

$$\phi_n = \frac{1}{n!} \left. \frac{d^n \phi(\omega)}{d\omega^n} \right|_{\omega=\omega_0} . \tag{2}$$

The first-, second-, and third-order derivatives are defined as group delay, group delay dispersion (GDD), and third-order dispersion (TOD), respectively. For most of the cases in ultrafast optics, higher-order dispersion than TOD is neglected since the effect on the pulse duration is relatively insignificant unless the pulse spectrum extends more than an octave. In this particular case, the OPA spectrum supports less than an octave. Therefore, only GDD and TOD will be considered in the dispersion management for the rest of the manuscript. GDD ($\phi_{2,mat.}$) and TOD ($\phi_{3,mat.}$) accumulated during the propagation of a pulse inside the material are calculated by the equations,

$$\phi_{2,mat.} = \frac{\lambda_0^3 L_m}{2\pi c^2} \left. \frac{d^2 n}{d\lambda^2} \right|_{\lambda=\lambda_0} \quad , \tag{3}$$

and

$$\phi_{3,mat.} = \left( \frac{\lambda_0^4}{4\pi c^3} \left. \frac{d^2 n}{d\lambda^2} \right|_{\lambda=\lambda_0} + \frac{\lambda_0^5}{12\pi^2 c^3} \left. \frac{d^3 n}{d\lambda^3} \right|_{\lambda=\lambda_0} \right) L_m \quad . \tag{4}$$

Here $\lambda_0$ is the carrier wavelength, $c$ is the speed of light in vacuum, $L_m$ is the propagation distance inside material, and $n$ is the refractive index of the material stated by the Sellmeier equation as a function of wavelength $(\lambda)$.

Figure 1 shows a simple Martinez-type grating stretcher where a telescope is placed between a grating pair which is mirror-symmetric of each other. In this particular Martinez grating stretcher, the telescope is configured as a 4-f imaging scheme in which the object and the image planes are behind gratings. Distances between the image plane and the gratings are chosen to be equal to the distance between the object plane and the grating $(L_g)$ for the sake of simplicity and symmetry, which allows employment of a mirror to make the stretcher compact. Here, two-pass geometry is assumed in which the beam is retroreflected after the first pass. The second-pass allows compensating spatial chirp originated from the first-pass. The associated GDD from the Martinez-type grating stretcher is calculated by the equation [32,36],

$$\phi_{2,str.} = \frac{m^2\lambda_0^3}{\pi c^2 d^2\left(1-\left(m\lambda_0/d-\sin\theta_i\right)^2\right)}L_p, \tag{5}$$

where $m$ is the order of the grating, $d$ is the groove spacing of the grating (1/groove density), $\theta_i$ is the incidence angle of the beam to the normal of the grating surface, and $L_p$ is the perpendicular distance between the image plane of the telescope and the gratings inside the Martinez stretcher. $L_p$ can be also expressed as $L_p = L_g/\cos\theta_d$ where $\theta_d$ is the diffraction angle from the grating and $L_g$ is the optical path length between the image plane of the telescope and the grating. TOD introduced by the grating stretcher is given by [32,36],

$$\phi_{3,str.} = -\phi_{2,str.}\frac{\lambda_0}{2\pi c}\left(1+\frac{m\lambda_0}{d}\left(\frac{m\lambda_0/d-\sin\theta_i}{1-\left(m\lambda_0/d-\sin\theta_i\right)^2}\right)\right). \tag{6}$$

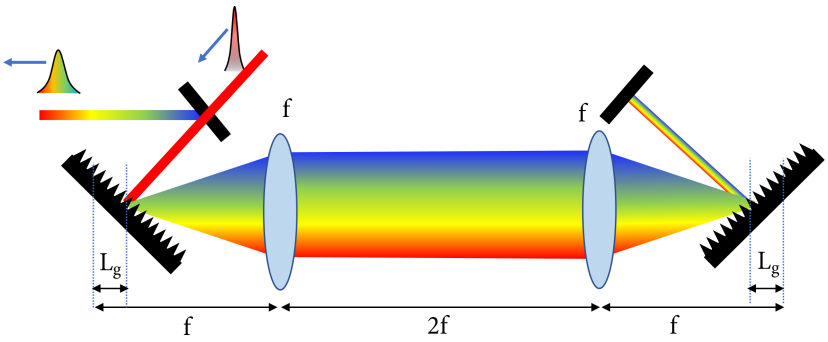


**Figure 1**. Sketch of Martinez-type grating stretcher.

### 2.3. Gain spectra of ZGP based OPAs

Figure 2 shows a model scheme of an OPA system in the MIR spectral region considered in this manuscript for dispersion management. As a driver pulse source, a Ho:YLF or Ho:YAG amplifier system is considered which can deliver pulses in the wavelength range of 2.05 and 2.09 µm with mJ-level pulse energy and few ps pulse

duration. Alternatively, Tm ion-doped solid-state amplifier systems would be considered but those amplifiers are not as mature as Ho doped systems due to low gain characteristics. The seed pulses are generated inside a 6-mm long YAG crystal (WL) via white-light continuum generation mechanism in a laser-driven filament which has been demonstrated before [39]. The generated pulses are stretched inside a Martinez grating stretcher to keep seed pulse comparable with the pump pulse duration. Here, the pump pulse duration is assumed to be between 1.8 and 2 ps, which is the typical pulse duration directly obtained from Ho:YLF amplifier systems without any additional pulse shaping during or before the amplification [40]. The seed pulse duration is kept between 1.4 and 1.6 ps which is 0.8 times the pump pulse duration in the amplification process. This ratio is considered for an efficient amplification without sacrificing the spectral bandwidth of the seed pulses in high gain OPAs and OPCPAs as proposed in [41]. The stretched pulses are amplified in a noncolinear OPA in two stages. As the parametric gain medium in OPAs, ZGP nonlinear crystal is employed, which provides the broadest bandwidth in MIR spectral region in noncolinear geometry among the other options such as CSP and GaS. Then the amplified pulses are compressed in a bulk material.

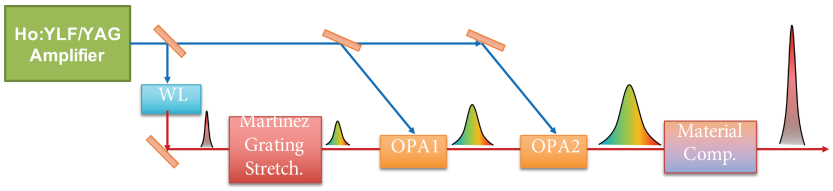


**Figure 2**. Model scheme for the OPA system.

Barium boron oxide (BBO) is a very common used nonlinear, negative uniaxial crystal (refractive index along the ordinary axis is larger than the extraordinary axis) for OPAs in the NIR spectral region. In standard BBO-based NIR OPAs, Type I phase matching in nonlinear geometry supports a very broadband spectrum. For instance, when BBO is pumped by the green pump pulses, the broadband phase-matching enables amplification of pulses with less than 10-fs transform-limited pulse duration [42]. For this particular phase-matching condition, the pump is polarized along an extraordinary axis and signal and idler beams are polarized along the ordinary axis of the crystal, whereas in the same phase-matching geometry for ZGP crystal, the pump is polarized along the ordinary axis and signal and idler beams are polarized along the extraordinary axis of the crystal due to positive uniaxial nature of the ZGP. Figure 3 (a) shows the phase-matching angle ($\theta$) in degrees for ZGP crystal for noncolinear angle ($\alpha$) of 3.67 degrees which provides the broadest bandwidth when it is pumped at 2.05 µm. The phase-matching angle is calculated by solving the equation numerically,

$$\frac{n_o(\lambda_p)}{\lambda_p} = \frac{n_e(\lambda_s,\theta)}{\lambda_s}\cos\alpha + \frac{n_e(\lambda_i,\theta)}{\lambda_i}\cos\beta, \tag{7}$$

where $n_o(\lambda_p)$ is the refractive index along the ordinary axis at the pump wavelength ($\lambda_p$), $n_e(\lambda_s\theta)$ is the refractive index along the extraordinary axis at the signal wavelength ($\lambda_s$), $n_e(\lambda_i\theta)$ is the refractive index along the extraordinary axis at the idler wavelength ($\lambda_i$), and $\beta$ is the angle between the pump and the idler wave vectors. As can be seen from Figure 3a, ZGP in noncolinear geometry provides a very broadband phase matching between 3 and 5 µm.

Gain spectrum of the OPAs is necessary to determine the dispersion parameters and figure out the transform-limited pulse duration. An analysis is conducted under the assumption of low pump depletion where

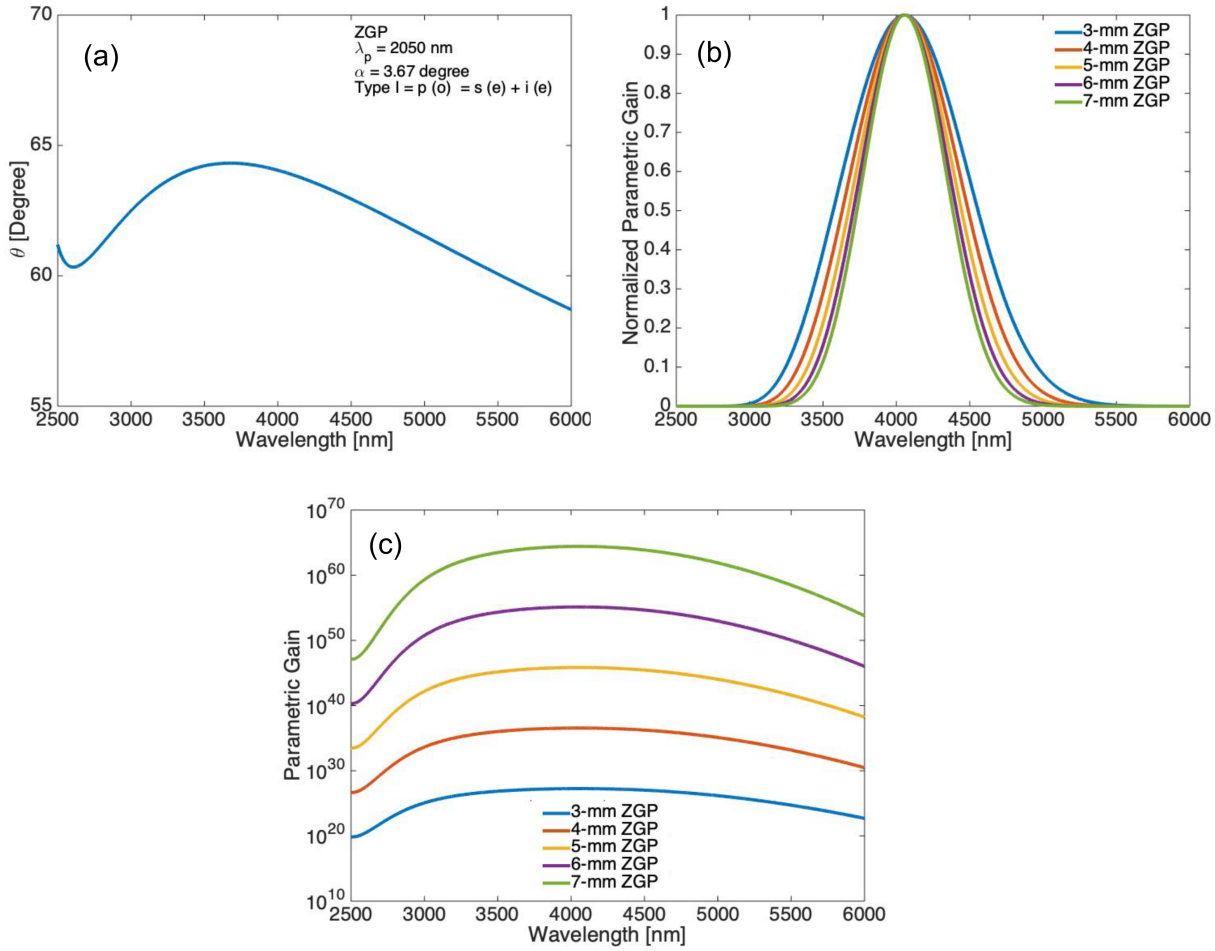


**Figure 3**. (a) Phase matching angle of ZGP, (b) Normalized gain spectra of ZGP-based OPA with different crystal thicknesses in noncolinear Type I phase matching configuration and (c) corresponding gain spectra in logarithmic scale.

the pump pulses are energetically significantly stronger than the signal pulses. During the analysis, a model described in [43] has been employed where the parametric gain ($G$) is defined by the equation,

$$G = 1 + \frac{^2}{g^2}\sinh^2(gL) \quad , \tag{8}$$

where

$$g = \sqrt{^2 - \frac{k^2}{4}}, \tag{9}$$

$$= \sqrt{\frac{8\pi^2 d_{eff}^2 I_p}{n_o(\lambda_p) n_e(\lambda_s,\theta) n_e(\lambda_i,\theta)\lambda_s\lambda_i\epsilon_0 c}}. \tag{10}$$

Here, $g$ is the nonlinear gain coefficient, $\Gamma$ is the nonlinear coefficient, $k$ is the phase mismatch of pump, signal and idler pulses, $d_{eff}$ is the effective nonlinear optical coefficient, $I_p$ is the pump intensity, and $\epsilon_0$ is the vacuum

permittivity. Figure 3b shows the normalized parametric gain of ZGP crystals with various thicknesses ranging from 3 to 7 mm to demonstrate the effect of the crystal thickness on the bandwidth of the amplified pulses. As can be seen, 3-mm-long crystal supports the broadest spectrum among the others with 26.5 fs (FWHM) transform limit pulses centered around 4.06 µm, whereas 7-mm-long crystal supports 38.1-fs long transform-limited pulses. However, 7-mm-long crystal provides 9 orders of magnitude more gain than 3-mm-long crystal under the same pump intensity as seen in the inset of Figure 3c.

## 3. Results and discussion

Figure 4a shows the necessary positive GDD from the stretcher to keep the seed pulse duration between 1.4 and 1.6 ps as a function of ZGP crystal thickness in each OPA except for 3-mm ZGP case, which will be discussed later. It should be noted that the crystal thickness is kept identical in both OPA stages to preserve the available bandwidth. As discussed in the previous section, gain bandwidth of the OPA decreases as the crystal length increases. To keep the pulse duration of the seed pulses in the targeted range (1.4–1.6 ps) for an efficient amplification in OPAs, the required chirp parameters (GDD and TOD) vary significantly depending on the OPA gain bandwidth. As the gain bandwidth decreases, the required GDD increases to get 1.4 to 1.6-ps pulses because in the narrow band case, there will be less frequency components inside the pulse and it requires higher delay between each spectral component to reach the same targeted pulse duration with respect to the broadband pulses. As shown in Figure 4a, the required GDD rises from 19600 to 24600 $fs^2$ to keep the seed pulse duration within the targeted range (1.4–1.6 ps). The contribution of positive GDD by ZGP crystals (OPAs, ranging from 1500 to 3500 $fs^2$) to the total GDD is very minor with respect to GDD from the stretcher. Besides, there is a constant GDD (–6900 $fs^2$) and TOD (58,600 $fs^3$) from the seed generation process for every OPA case which corresponds to 6-mm propagation inside YAG. The amount of required negative GDD from the compressor increases from –14200 to –21200 $fs^2$ to balance the total dispersion. As a reminder, in the dispersion management scheme, bulk compression is preferred due to low optical losses of the materials. In particular, $CaF_2$ is preferred as the bulk compressor due to relatively low TOD-to-GDD ratio and availability of the material with large quantities and very good optical quality. As can be seen from the figure, to compress the pulses, the required propagation distance in $CaF_2$ grows linearly from 47 to 72 mm since the necessary GDD also increases linearly. It should be noted that there is no fundamental physical reason preventing the use of sapphire or $LiNbO_2$ in the compression.

To compresses the pulses without any significant pedestals, TOD also needs to be balanced at the end of compression. Figure 4b shows the TOD of the compressor ($CaF_2$) and OPAs (two ZGP crystals) for different ZGP thicknesses. As can be seen, the compressor has relatively high positive TOD with respect to OPAs and rises linearly from 101400 to 152000 $fs^3$ as a function of ZGP crystal thickness since the required material propagation length increases as a function of ZGP crystal thickness. The ratio between TOD and GDD of the materials is not a tunable parameter. Hence, TOD from the stretcher will be adjusted to match the residual TOD accordingly ranging from –169,200 to –228,800 $fs^3$ as shown in the figure. For compression of the pulses, the necessary TOD-to-GDD ratio in the stretcher is demonstrated as a function of the ZGP crystal length in Figure 5a. As illustrated, the ratio linearly decreases from –8.63 to –9.31 fs as the ZGP crystal thickness increases from 3 to 7 mm. This range can be covered by tuning the incidence angle of the Martinez grating pair. The ratio of TOD-to-GDD from the grating pair is an independent parameter of $L_g$ which is used to balance the ratio of total TOD to GDD contributed by the seed, OPAs, and the compressor. In Figure 5b, the TOD-to-GDD ratio of the Martinez grating pair is presented as a function of incidence angle for 5 different

grating pairs with groove density ranging from 50 to 200 lines/mm. Besides, the corresponding blaze angle for each grating is shown to provide indirect information about the efficiency of the grating stretcher. As a side note, for blazed gratings, the deviation of the incidence angle from the blaze angle results in a reduction of the diffraction efficiency. In this particular dispersion management scheme, the efficiency of the stretcher is not a critical parameter since the loss can be simply compensated in the first OPA stage. In the figure, the red shaded area shows the range of required TOD-to-GDD ratio from the stretcher. As illustrated, any of the grating pair can be tuned to provide the required ratio from the stretcher for this two-stage OPA system with any ZGP crystal involved.

Figure 6a shows the calculated optical path length between the image plane of the lens and the grating ($L_g$) inside the Martinez grating stretcher for different OPA cases with various ZGP crystal thicknesses as a function of grating groove density. It should be noted that, for each case, TOD of the stretcher is tuned to match the total TOD introduced by OPAs (two ZGP crystals), the seed (6mm-YAG), and the compressor ($CaF_2$ crystal). As can be seen, when the groove density increases from 50 to 200 lines/mm, the required $L_g$ decreases very significantly from ~15 to ~2 mm as expected because the angular dispersion of grating grows rapidly as a function of groove density resulting in the rise of GDD and TOD of the grating pair. The stretcher, which comprises a grating pair with groove density of 200 lines/mm, provides necessary GDD and TOD with only ~2 mm of $L_g$. That will lead to a compact stretcher design but with a price of alignment sensitivity. As can be seen in the figure, the OPA crystal length has only a slight effect on the required $L_g$ for the compression which is hardly seen. To demonstrate this effect, the optical path length between the image plane of the lens and the grating is plotted as a function of ZGP crystal thickness in OPAs in Figure 6b. Here the stretcher is based on a grating pair with a groove density of 75 lines/mm. As can be seen, to compensate for the dispersion for 3-mm ZGP case, only 8.6 mm $L_g$ is needed, whereas for 7-mm ZGP case, the required $L_g$ increases only by 0.5 mm to 9.1 mm.

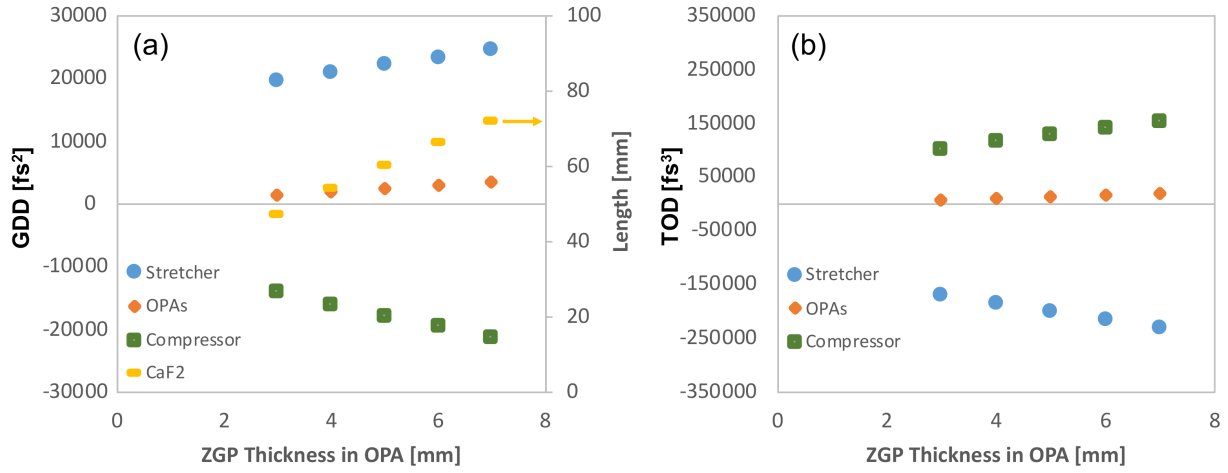


**Figure 4**. (a) GDD and (b) TOD of stretcher, OPAs and compressor for OPA schemes based on ZGP crystals with different thicknesses. (a) Required propagation distance in $CaF_2$ to compress the pulses for OPA schemes of various thicknesses.

Figure 7 demonstrates the transform-limited pulses and the pulse evolution inside the model OPA system for three different ZGP crystal thicknesses (3, 5, and 7 mm). Residual GDD and TOD over the pulse during the propagation are noted on the graphs for each step of the evolution. 3-, 5-, and 7-mm ZGP crystal-based

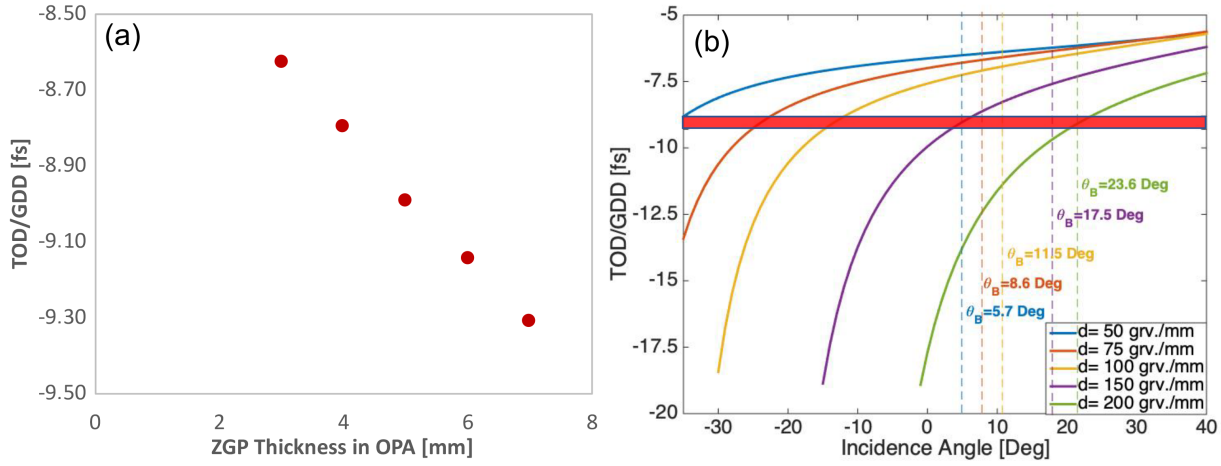


**Figure 5**. (a) Required TOD/GDD for a stretcher for OPAs as a function of ZGP crystals' thicknesses. (b) Ratio of TOD to GDD of a Martinez-type grating stretcher as a function of incidence angle for the gratings with various groove densities between 50 to 200 groove/mm and corresponding blaze angles.

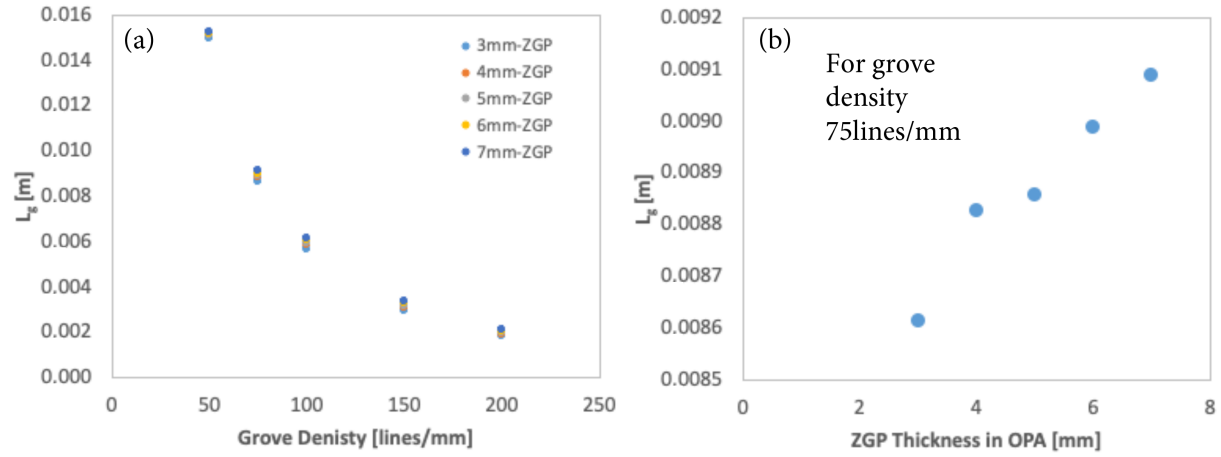


**Figure 6**. (a) Required optical path length from the image point of the lens to the second grating position in Martinez grating stretcher as a function of groove density for OPA configuration with various ZGP thicknesses. (b) The optical path length from the image point of the lens to the second grating position in Martinez grating stretcher as a function of ZGP crystals' thicknesses for the groove density 75 lines per mm.

OPAs support pulses with 26.5, 32.8, and 38.1 fs (FWHM) pulses, respectively. As the seed pulses are generated inside the YAG crystal, they have stretched to ~510 fs (FWHM) due to propagation in the material. GDD and TOD accumulated during pulse propagation inside YAG crystal are slightly different for each case due to a minor change of the carrier wavelength supported by each OPA crystal. GDD varies between –6880 and –7010 $fs^2$ and TOD changes between 58200 and 59800 $fs^3$. Here, it is assumed that all the spectral components are generated almost at the beginning of the YAG crystal during the white-light continuum generation. This can vary slightly depending on the white-light generation conditions [39]. However, this slight change has a very minor effect on the analysis demonstrated in this manuscript. As can be seen for 3-mm ZGP case, TOD leads ripples at the leading or falling edge of the pulse (depending on the sign), whereas TOD becomes less effective

as the crystal length increases due to a decrease in the bandwidth of the pulse. After the Martinez grating stretcher, both GDD and TOD change the sign and hence the place of the tipples for the stretched pulses.

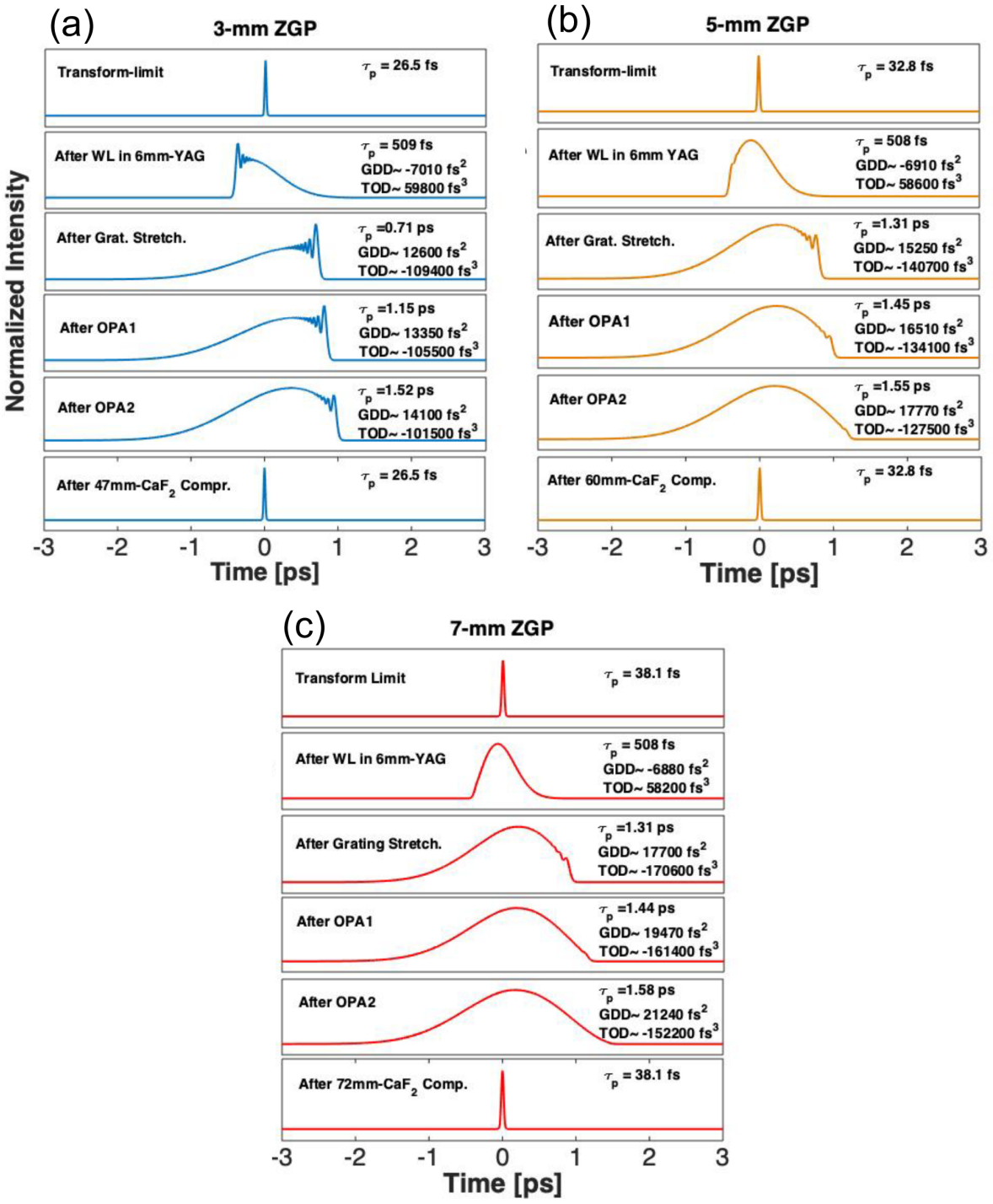


**Figure 7**. Pulse evolution inside the OPA system for (a) 3-mm, (b) 5-mm, and (c) 7-mm ZGP OPA cases. The groove density of the grating is 75 lines per mm for all cases.

As mentioned earlier, during the amplification inside OPA stages, the pulse duration is kept between 1.4 and 1.6 ps (FWHM) to reduce the walk-off between pump and signal for an efficient amplification expect for 3-mm ZGP case. Here, GDD and TOD from the ZGP crystals in OPAs are sufficient enough to stretch the pulses beyond the targeted pulse duration range in the OPAs because of the relatively large bandwidth with respect to the other OPA cases. For 3-mm ZGP case, the pulse duration is kept 1.15 ps after the first OPA stage, and then the pulses are stretched to 1.52 ps after the second OPA stage. As a side note, the groove density of the grating pair is chosen to be 75 lines per mm for all cases. Finally, pulses are compressed to the transform limit after the propagation inside $CaF_2$ with thicknesses 47, 60, and 72 mm for 3-, 5-, and 7-mm ZGP OPA cases, respectively.

## 4. Summary

In this manuscript, a dispersion management schemes for OP(CP)As in MIR spectral region is proposed and numerically analyzed. Then the scheme is applied numerically to a 2-µm pumped, two-stage ZGP-based OPA system at 4.06 µm. In order to estimate the transform-limited pulse duration and fix the parameters in the dispersion management, parametric gain bandwidth of the ZGP nonlinear crystal is numerically studied for crystal thicknesses varying between 3 and 7 mm. Simulations suggested that 3-mm ZGP crystal potentially provides pulses with 26.5 fs pulse duration (FWHM) at 4.06 µm. With the proposed dispersion management scheme, the seed pulses are first stretched to 1.4–1.6 ps inside a Martinez grating stretcher for efficient amplification in OPA stages. After the amplification, the pulses are compressed to the transform-limit inside $CaF_2$ bulk material. As a next step, the proposed dispersion management will be implemented experimentally to demonstrate the shortest possible pulses from an OPA/OPCPA in the MIR spectral region.

## Acknowledgments

The author acknowledges Franz X. Kaertner and Ümit Demirbaş.

## References

[1] Pires H, Baudisch M,Sanchez D, Hemmer M, Biegert J. Ultrashort pulse generation in the mid-IR. Progress in Quantum Electronics 2015; 43: 1-30. doi: 10.1016/j.pquantelec.2015.07.001

[2] Blaga CI,Catoire F,Colosimo P,Paulus GG,Muller HG et al. Strong-field photoionization revisited. Nature Physics 2009; 5 (5): 335-338. doi: 10.1038/Nphys1228

[3] Dura J, Camus N,Thai A,Britz A, Hemmer M et al. Ionization with low-frequency fields in the tunneling regime. Scientific Reports 2013; 3. doi:ARTN 267510.1038/srep02675

[4] Ludwig A, Maurer J, Mayer BW, Phillips CR, Gallmann L et al. Breakdown of the dipole approximation in strong-field ionization. Physical Review Letters 2014; 113 (24). doi:ARTN 24300110.1103/PhysRevLett.113.243001

[5] Colosimo P, Doumy G, Blaga CI, Wheeler J, Hauri C et al. Scaling strong-field interactions towards the classical limit. Nature Physics 2008; 4 (5): 386-389. doi: 10.1038/nphys914

[6] Deloach LD, Page RH , Wilke GD,Payne SA, Krupke WF. Transition metal-doped zinc chalcogenides: Spectroscopy and laser demonstration of a new class of gain media. IEEE Journal of Quantum Electronics 1996; 32 (6): 885-895. doi: 10.1109/3.502365

[7] Sorokin E, Naumov S , Sorokina IT. Ultrabroadband infrared solid-state lasers. IEEE Journal of Selected Topics in Quantum Electronics 2005; 11 (3): 690-712. doi: 10.1109/Jstqe.2005.850255

[8] Mirov SB, Fedorov VV, Martyshkin DV, Moskalev IS, Mirov MS et al. Progress in mid-IR $Cr^{2+}$ and $Fe^{2+}$ doped II-VI materials and lasers. Optical Materials Express, 2011; 1 (5): 898-910. doi: 10.1364/OME.1.000898

[9] Demirbas U,Sennaroglu A.Intracavity-pumped $Cr^{2+}$: ZnSe laser with ultrabroad tuning range between 1880 and 3100 nm. Optics Letters 2006; 31 (15): 2293-2295. doi: 10.1364/Ol.31.002293

[10] Pollock CR, Brilliant NA, Gwin D, Carrig TJ, Alford WJ et al. Mode locked and Q-switched Cr:ZnSe laser using a semiconductor saturable absorbing mirror (SESAM). In: Advanced Solid-State Photonics (TOPS). 2005. Vienna: Optical Society of America.

[11] Sorokina IT, Sorokin E, Carrig TJ , Schaffers KI. A SESAM passively mode-locked Cr:ZnS laser. In: Advanced Solid-State Photonics. 2006. Incline Village, Nevada: Optical Society of America.

[12] Sorokina IT, Sorokin E, Carrig T. Femtosecond pulse generation from a SESAM Mode-Locked Cr:ZnSe laser. In: Conference on Lasers and Electro-Optics/Quantum Electronics and Laser Science Conference and Photonic Applications Systems Technologies. 2006. Long Beach, California: Optical Society of America.

[13] Cizmeciyan MN, Cankaya H, Kurt A, Sennaroglu A. Kerr-lens mode-locked femtosecond $Cr^{2+}$:ZnSe laser at 2420 nm. Optics Letters, 2009; 34 (20): 3056-3058. doi: 10.1364/OL.34.003056

[14] Tolstik N, Sorokin E, Sorokina IT. Kerr-lens mode-locked Cr:ZnS laser. Optics Letters 2013; 38 (3): 299-301. doi: 10.1364/OL.38.000299

[15] Sorokin E, Tolstik N, Sorokina IT. Femtosecond operation and self-doubling of Cr:ZnS laser. In: Nonlinear Optics. 2011. Kauai, Hawaii: Optical Society of America.

[16] Hemmer M, Thai A, Baudisch M, Ishizuki H , Taira T et al. 18- µJ energy, 160-kHz repetition rate, 250-MW peak power mid-IR OPCPA. Chinese Optics Letters 2013; 11 (1): 013202.

[17] Andriukaitis G, Balčiūnas T, Ališauskas S, Pug lys A, Baltuška A et al. 90 GW peak power few-cycle mid-infrared pulses from an optical parametric amplifier. Optics Letters 2011; 36 (15): 2755-2757. doi: 10.1364/OL.36.002755

[18] Zhao K, Zhong H , Yuan P , Xie G, Wang J et al. Generation of 120 GW mid-infrared pulses from a widely tunable noncollinear optical parametric amplifier. Optics Letters 2013; 38 (13): 2159-2161. doi: 10.1364/OL.38.002159

[19] Petrov V, Parametric down-conversion devices: The coverage of the mid-infrared spectral range by solid-state laser sources. Optical Materials 2012;34 (3): 536-554. doi: 10.1016/j.optmat.2011.03.042

[20] Malevich P, Andriukaitis G, Flory T, Verhoef AJ, Fernandez A et al. High energy and average power femtosecond laser for driving mid-infrared optical parametric amplifiers. Optics Letters, 2013; 38 (15): 2746-2749. doi: 10.1364/Ol.38.002746

[21] Phillips CR, Jiang J, Mohr C, Lin AC, Langrock C et al.Widely tunable midinfrared difference frequency generation in orientation-patterned GaAs pumped with a femtosecond Tm-fiber system. Optics Letters 2012; 37 (14): 2928-2930. doi: 10.1364/OL.37.002928

[22] Elu U,Steinle T, Sanchez D, Maidment L, Zawilski K et al. Table-top high-energy 7 µm OPCPA and 260 mJ Ho:YLF pump laser. Optics Letters 2019; 44 (13): 3194-3197. doi: 10.1364/Ol.44.003194

[23] von Grafenstein L, Bock M, Griebner U, Elsaesser T. High-energy multi-kilohertz Ho-doped regenerative amplifiers around 2 µm. Optics Express 2015; 23 (11): 14744-14752. doi: 10.1364/Oe.23.014744

[24] von Grafenstein L, Bock M, Ueberschaer D, Griebner U, Elsaesser T. Ho:YLF chirped pulse amplification at kilohertz repetition rates-4.3 ps pulses at 2 µm with GW peak power. Optics Letters 2016; 41 (20): 4668-4671. doi: 10.1364/Ol.41.004668

[25] Malevich P, Kanai T, Hoogland H, Holzwarth R, Baltuska A et al. Broadband mid-infrared pulses from potassium titanyl arsenate/zinc germanium phosphate optical parametric amplifier pumped by Tm, Ho-fiber-seeded Ho:YAG chirped-pulse amplifier. Optics Letters 2016; 41(5): 930-933. doi: 10.1364/Ol.41.000930

[26] Sanchez D, Hemmer M, Baudisch M, Cousin SL, Zawilski K et al. 7 µm, ultrafast, sub-millijoule-level mid-infrared optical parametric chirped pulse amplifier pumped at 2 µm. Optica 2016; 3 (2): 147-150. doi: 10.1364/Optica.3.000147

[27] Bock M, von Grafenstein L, Griebner U, Elsaesser T. Generation of millijoule few-cycle pulses at 5 µm by indirect spectral shaping of the idler in an optical parametric chirped pulse amplifier. Journal of the Optical Society of America B-Optical Physics 2018; 35 (12): C18-C24. doi: 10.1364/Josab.35.000c18

[28] Fork RL, Martinez OE, Gordon JP. Negative dispersion using pairs of prisms. Optics Letters 1984; 9 (5): 150-152. doi: 10.1364/OL.9.000150

[29] Fork RL, Brito Cruz CH, Becker PC, Shank CV. Compression of optical pulses to six femtoseconds by using cubic phase compensation. Optics Letters 1987; 12 (7): 483-485. doi: 10.1364/OL.12.000483

[30] Szipöcs R, Ferencz K, Spielmann C, Krausz F. Chirped multilayer coatings for broadband dispersion control in femtosecond lasers. Optics Letters 1994; 19 (3): 201-203. doi: 10.1364/OL.19.000201

[31] Stingl A, Lenzner M, Spielmann C, Krausz F, Szipöcs R. Sub-10-fs mirror-dispersion-controlled Ti:sapphire laser. Optics Letters 1995; 20 (6): 602-604. doi: 10.1364/OL.20.000602

[32] Kane S, Squier J. Grism-pair stretcher–compressor system for simultaneous second- and third-order dispersion compensation in chirped-pulse amplification. Journal of the Optical Society of America B 1997; 14 (3): 661-665. doi: 10.1364/JOSAB.14.000661

[33] Tournois P. New diffraction grating pair with very linear dispersion for laser pulse compression. Electronics Letters 1993; 29 (16): 1414-1415. doi: 10.1049/el:19930947

[34] Weiner AM. Femtosecond pulse shaping using spatial light modulators. Review of Scientific Instruments 2000; 71 (5): 1929-1960. doi: 10.1063/1.1150614

[35] Verluise F, Laude V, Cheng Z, Spielmann C, Tournois P. Amplitude and phase control of ultrashort pulses by use of an acousto-optic programmable dispersive filter: pulse compression and shaping. Optics Letters 2000; 25 (8): 575-577. doi: 10.1364/OL.25.000575

[36] Martinez O. 3000 times grating compressor with positive group velocity dispersion: Application to fiber compensation in 1.3-1.6 µm region. IEEE Journal of Quantum Electronics 1987; 23 (1): 59-64. doi: 10.1109/JQE.1987.1073201

[37] Sherriff RE. Analytic expressions for group-delay dispersion and cubic dispersion in arbitrary prism sequences. Journal of the Optical Society of America B 1998; 15 (3): 1224-1230. doi: 10.1364/JOSAB.15.001224

[38] Kane S, Squier J. Grating compensation of third-order material dispersion in the normal dispersion regime: Sub-100-fs chirped-pulse amplification using a fiber stretcher and grating-pair compressor. IEEE Journal of Quantum Electronics, 1995; 31 (11): 2052-2057. doi: 10.1109/3.469287

[39] Calendron AL, Cankaya H, Cirmi G, Kärtner FX. White-light generation with sub-ps pulses. Optics Express 2015; 23 (11): 13866-13879. doi: 10.1364/Oe.23.013866

[40] Murari K, Cankaya H, Kroetz P, Cirmi G, Li P et al. Intracavity gain shaping in millijoule-level, high gain Ho:YLF regenerative amplifiers. Optics Letters 2016; 41 (6): 1114-1117. doi: 10.1364/OL.41.001114

[41] Moses J, Manzoni C, Huang SW, Cerullo G, Kartner FX. Temporal optimization of ultrabroadband high-energy OPCPA. Optics Express 2009; 17 (7): 5540-5555. doi: 10.1364/Oe.17.005540

[42] Çankaya H, Calendron AL, Zhou C, Chia SH, Mücke OD et al. 40-$\mu$J passively CEP-stable seed source for ytterbium-based high-energy optical waveform synthesizers. Optics Express 2016; 24 (22): 25169-25180. doi: 10.1364/OE.24.025169

[43] Cerullo G,De Silvestri S. Ultrafast optical parametric amplifiers. Review of Scientific Instruments 2003; 74 (1): 1. doi: 10.1063/1.1523642

[44] Georgiev G, Glenar DA,Hillman JJ. Spectral characterization of acousto-optic filters used in imaging spectroscopy. Applied Optics 2002; 41 (1): 209-217.

[45] Zelmon DE, Small DL, Page R. Refractive-index measurements of undoped yttrium aluminum garnet from 0.4 to 5.0 µm. Applied Optics 1998; 37 (21): 4933-4935. doi: 10.1364/Ao.37.004933

[46] Connolly J, diBenedetto B, Donadio R. Specifications Of Raytran Material. Technical Symposium East. Vol. 0181. 1979: SPIE.

[47] Chandler-Horowitz D, Amirtharaj PM. High-accuracy, midinfrared (450 $\mathrm{cm}^{-1}$ <=omega <= 4000 $\mathrm{cm}^{-1}$) refractive index values of silicon. Journal of Applied Physics 2005; 97 (12). doi: 12352610.1063/1.1923612

[48] Zelmon DE, Small DL, Jundt D. Infrared corrected Sellmeier coefficients for congruently grown lithium niobate and 5 mol. % magnesium oxide-doped lithium niobate. Journal of the Optical Society of America B-Optical Physics, 1997. 14 (12): p. 3319-3322. doi:Doi 10.1364/Josab.14.003319

[49] Malitson IH, Dodge MJ. Refractive-index and birefringence of synthetic sapphire. Journal of the Optical Society of America 1972; 62 (11): 1405-1405. doi: 10.1364/JOSA.52.001377

[50] Burnett J, Kaplan S, Stover E, Phenis A. Refractive index measurements of Ge. SPIE Optical Engineering + Applications. Vol. 9974. 2016: SPIE.

[51] Li HH. Refractive-index of alkaline-earth halides and its wavelength and temperature derivatives. Journal of Physical and Chemical Reference Data 1980; 9 (1): 161-289. doi:Doi 10.1063/1.555616

[52] Dodge MJ. Refractive Properties of magnesium fluoride. Applied Optics 1984; 23 (12): 1980-1985. doi: 10.1364/Ao.23.001980

[53] Das S,Bhar GC, Gangopadhyay S, Ghosh C. Linear and nonlinear optical properties of $ZnGeP_2$ crystal for infrared laser device applications: revisited. Applied Optics 2003; 42 (21): 4335-4340. doi: 10.1364/Ao.42.004335